Available online at www.sciencedirect.com
SCIENCE DIRECT®
ELSEVIER
International Journal of Impact Engineering 30 (2004) 1333–1351
INTERNATIONAL JOURNAL OF IMPACT ENGINEERING
www.elsevier.com/locate/ijimpeng

Explosive welding of aluminum to aluminum: analysis, computations and experiments

F. Grignon, D. Benson, K.S. Vecchio, M.A. Meyers*

Department of Mechanical and Aerospace Engineering, University of California, San Diego, La Jolla, CA 92093-0411, USA

Received 11 November 2002; accepted 23 September 2003

Dedicated to Professor Werner Goldsmith

Abstract

6061 T0 aluminum alloy was joined to 6061 T0 aluminum alloy by explosive welding. This is a process in which the controlled energy of a detonating explosive is used to create a metallic bond between two similar or dissimilar materials. The welding conditions were tailored to produce both wavy and straight interfaces.

A three-pronged study was used to establish the conditions for straight weld formation: (a) analytical calculation of the domain of weldability, in which the Szecket–Mayseless (Mater. Sci. Eng. 57 (1983) 149) criterion was successfully used; (b) characterization of the explosive welding experiments carried out under different conditions, and (c) 2D finite differences simulation of these tests using the explicit Eulerian hydrocode Raven with a Johnson–Cook constitutive equation for the Al alloy. The numerical simulation and the analytical calculations confirm the experimental results and explain the difficulties met for obtaining a continuous straight interface along the entire weld.
Published by Elsevier Ltd.

Keywords: Explosive welding; Aluminum; Experiments; Numerical simulations; Wavy-smooth transition

1. Introduction

The Mars Sample Return Mission planned for the future will use a capsule to collect soil samples. This capsule will be hermetically sealed on Mars prior to the return mission in order to avoid contamination upon return to Earth. A novel containerization technique that satisfies the Planetary Protection Category V requirements has been developed at the Jet Propulsion

*Corresponding author. Tel.: +619-534-4719; fax: +619-534-7078.
E-mail address: mameyers@mae.ucsd.edu (M.A. Meyers).

0734-743X/$ - see front matter Published by Elsevier Ltd.
doi:10.1016/j.ijimpeng.2003.09.049

Laboratory [1]. The proposed approach uses explosive welding, which possesses several characteristics that are important for the planetary protection compliant containerization:

1. The weld formed is based on the metallic bond; thus, the seam behaves like a bulk metal, i.e., it constitutes a bio-barrier.

2. The weld is very tolerant of contamination and thus has an extremely low probability of failure and a high tolerance of the pre-welding contamination.

3. The surface cleaning is a mechanical process that does not use external tools that may be contaminated.

The contaminants are stripped away by a very energetic process. This is the jet, that is generated at the impacting surfaces. In addition, there are indications that the conditions of welding may be capable of destroying any carbon–carbon based chemistry and, thus, perform verifiable sterilization of even unknown life. The main disadvantages of the explosive welding process, from a planetary protection point of view, are the small thickness of the stripped layer and the propensity of the bond to form interface waves that may prevent ejecta from completely leaving the bonded area and trap some surface particles within these waves.

It is known that the quality and morphology of the interface depend on the collision angle, the impact velocity, the properties of the materials, and the geometry of the welded plates. The objective of the research program whose results are described herein, was to determine the right parameters for providing the smoothest interface. The development of a theoretical model that is capable of describing the mechanism by which waves are produced is the soundest approach and was implemented herein.

Consequently, the first part of the study consisted of utilizing the recent advances in the domain of explosive welding to develop an analytical understanding. The hydrodynamic analogy has been frequently used for the prediction of the wave properties, but dynamic plasticity plays a significant role. This enables the establishment of experimental conditions for the formation of the wavy and smooth interfaces.

The second part of the study consisted of characterizing explosive welds carried out with different initial configurations. The initial angle between the plates, α, was varied from 4° to 14° in 2° increments.

The third part of the study consisted of utilizing Raven, an explicit multi-material Eulerian finite element program. Raven was developed for solving dynamics problems in solid mechanics and materials science with an emphasis on the micromechanical aspects. The first step is the simulation of the experimental tests performed by the Jet Propulsion Laboratory. All the calculations were performed in 2D to reach the best equilibrium between quantity, rapidity, reliability, and quality.

The origins of explosive welding are close to ballistic effects: the explosive welding mechanism is very similar to the shaped charge mechanism described by Birkhoff [2]. Deribas [3] and Crossland [4] wrote complete monographs on the process and a large number of scientists worked on the understanding of the subject [2–26]. The parallel plate configuration (see Fig. 1), in which the welding velocity is equal to the detonation velocity, illustrates the principal aspects of the process. The initial angle α between the two plates is zero since they are parallel. The collision angle β is obtained from the collision and plate velocities by simple geometrical considerations. A geometrical analysis [5] shows that the plate velocity bisects the angle between the initial plate and

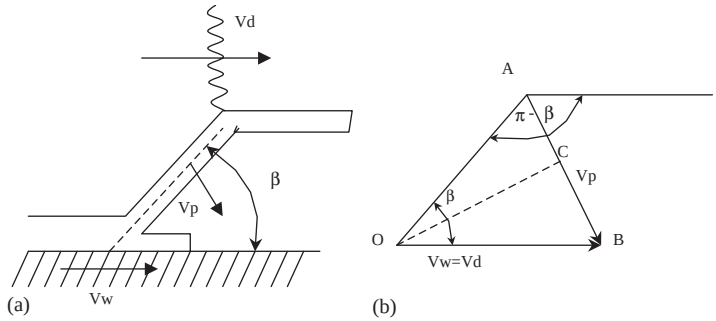

Fig. 1. (a) Mechanism of explosive welding (parallel configuration); (b) geometrical analysis.

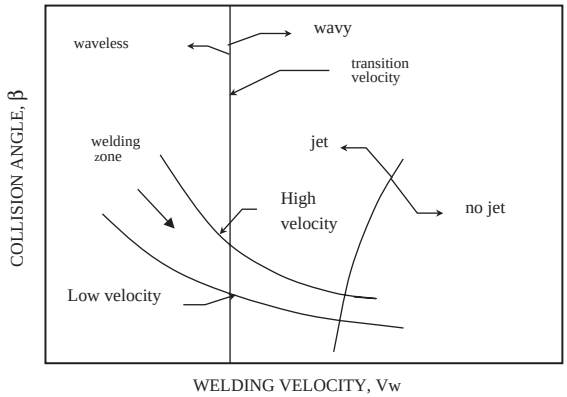

Fig. 2. Theoretical and practical boundaries for wave formation and jetting [6,7].

the deformed plate orientations. On a per unit of time basis, A goes to B with V_p when point O goes to B with V_w. Triangle OAB is isosceles; for triangle OBC one has

$$1/2V_p = V_d \sin(\beta/2). \tag{1}$$

When $\beta < 10^\circ$, one can use the approximation $V_p \cong V_d \sin\beta$.

β and V_p are the most important parameters of explosive welding. The formation of a jet is a necessary prerequisite for explosive welding.

Wittman [6] and Deribas [7] developed an explosive welding window (Fig. 2), in which the collision angle β is plotted in the ordinates and the welding velocity, V_w, is plotted in the abscissa. They studied jet formation, the critical impact pressure, the maximum impact velocity and wavy–smooth transition velocity. For example, if V_w reaches a supersonic value, there is no jetting. The same happens if the impact pressure is too low. The wavy–smooth transition parameter does not appear in this plot and needs to be studied more closely.

2. Analysis

2.1. The smooth–wavy transition

A model capable of predicting the wave geometry would be able to determine the smooth–wavy transition. Deribas [8] developed the first model, based on experimental results. It is a hydrodynamic model, which describes wave formation as being analogous to fluid flow behind an obstacle. Thus, the smooth–wavy boundary corresponds to the laminar-turbulent transition. In fluid mechanics the Reynolds number characterizes this transition. Cowan et al. [9,10] introduced the following Reynolds number R_t for explosive welding:

$$R_t = (\rho_a + \rho_b)V_t^2/2(H_a + H_b), \tag{2}$$

where ρ_a and ρ_b are the densities of the materials and H_a and H_b are their Vickers hardnesses.

This new parameter was an important advance in the domain, but the hydrodynamic analogy contained limitations reported by Jaramillo and Szecket [11]. In the hydrodynamic model, the waves generated behind an obstacle reach a stable configuration after a certain distance while the waves at the weld interface must be created at the collision point. Furthermore, even if the fluid analogy applies to the collision point, what kind of fluid is assumed and what is the response of the regions removed from this area? Nevertheless, Cowan et al. [10] obtained correct results with regard to the smooth–wavy transition. In all of their experiments, Eq. (2) in which R_t is equal to 10.6 describes the transition very well. The limitation is that they studied only one collision angle, $\beta = 12^\circ$. This relationship is not applicable for a generic collision angle. In order to generalize, it is necessary to obtain a relationship between the Reynolds number and the collision angle. A model was developed by Szecket [11–15] for the three following material couples: Fe–Fe, Cu–Cu, Al–Al (2024 Al alloy) (Flyer plate thickness: 3.2 mm). When all the data for these three different systems are combined, the following general relationship between the Reynolds number and the collision angle is obtained with a correlation factor = 0.9853:

$$R_t = K_{EP} = 93.02(\pm 9.62) - 13.45(\pm 2.06)\beta + 0.71(\pm 0.14)\beta^2 - 0.012(\pm 0.03)\beta^3. \tag{3}$$

Eq. (3) provides a very good approximation of the smooth–wavy transition for the systems studied. This equation is the first step toward a dynamic plasticity model and implies to redefine R_t by the elastic–plastic constant K_{EP}.

2.2. Weldability window

The advances achieved by Deribas [3], Wittman [6], Cowan [9] and Szecket [12] enable the construction of a plot that Szecket named the ''weldability window'', which includes both a straight and wavy interface domain. This plot is applied to the 6061 T0 aluminum alloy used in this investigation. The appropriate equations for the inclined plate configuration used in this investigation are presented next. The establishment of a weldability window requires the relationship between the initial conditions (the initial angle α and the characteristics of the explosive) and the collision angle β. The geometrical considerations applied to this configuration

give the following equations [4]:

$$\sin\left(\frac{\beta-\alpha}{2}\right)=\frac{V_p}{2V_d}, \tag{4}$$

$$V_w=\frac{V_p}{\sin\beta}\cos\left(\frac{\beta-\alpha}{2}\right), \tag{5}$$

$$V_f=\frac{V_p}{\sin\beta}\cos\left(\frac{\beta+\alpha}{2}\right). \tag{6}$$

Knowing α, V_p and V_d, β can be obtained from Eq. (1). V_p is calculated from the Gurney equation [26,27] for the specific explosive welding geometry

$$V_p=\sqrt{2E}\left(\frac{(1+2/R)^3+1}{6(1+1/R)}+\frac{1}{r}\right)^{-1/2}. \tag{7}$$

$R=C/M$ is the mass of explosive for unit mass of flyer plate. $\sqrt{2E}$ is the Gurney energy, which is experimentally known for common explosives. The Gurney equation only predicts a terminal velocity; the problem of the flyer plate acceleration is intentionally left out. V_w and V_f can be calculated by Eqs. (5) and (6). Known values of α, β, V_d, V_p, V_f, V_w and the properties of the material enable the design of the weldability window. This diagram can be drawn in both the V_w vs. β and V_p vs. β plane. Eq. (8) gives the lower limit for welding (due to Deribas et al. [8]). In Eq. (8), β is in radians, k_1 is a constant, H is the Vickers hardness in N/m^2, and ρ is the density in kg/m^3. The value of k_1 is 0.6 for high-quality

$$\beta=k_1\sqrt{\frac{H}{\rho\cdot V_w^2}} \tag{8}$$

pre-cleaning of surfaces, and 1.2 for imperfectly cleaned surfaces.

Eq. (9), due to Deribas [8] and Wittman [7], gives the upper limit for welding. k_3 should be evaluated experimentally at a value of V_w, which is equal to half of the compressive wave velocity C_f ($V_w=2645$ m/s for pure aluminum); t is the thickness of the flyer plate:

$$\sin\frac{\beta}{2}=\frac{k_3}{t^{0.25}V_w^{1.25}}, \tag{9}$$

where $k_3=C_f/2$, $C_f=\sqrt{K/\rho}$, $K=E/3(1-2\,v)$.

Eq. (10), due to Szecket [11], gives the smooth–wavy transition zone for the 2024 Al alloy. This zone has been built with experimental results.

$$\begin{aligned}&\text{For Al}-\text{Al 2024}:\\&R_t=122.32(\pm16.9)-19.35(\pm3.65)\beta+1.07(\pm0.24)\beta^2-0.020(\pm0.005)\beta^3,\\&\text{correlation factor}=0.9939.\end{aligned} \tag{10}$$

Szecket [12] developed a weldability zone, which contained left and right boundaries. His results for 2024 Al will be merged with data for the 6061 T0 aluminum alloy used in this investigation. Specific parameters are: $\rho=2700\,kg/m^3$; $H_v=38\,kg/mm^2$; $C_f=5293$ m/s.

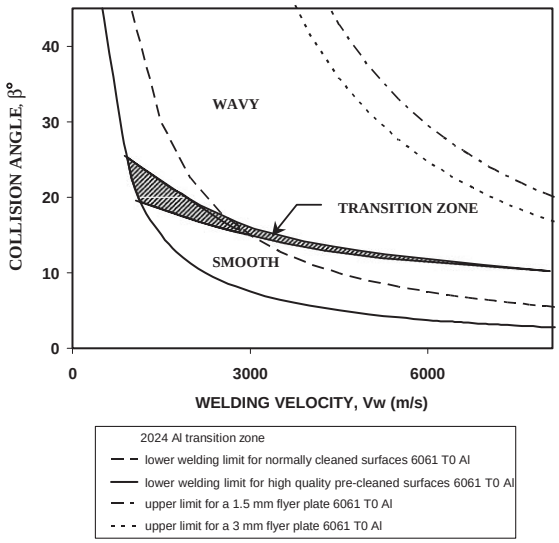

Fig. 3. Weldability window of the 6061 T0 aluminum alloy. Upper and lower limits due to Deribas [7], wavy–smooth transition due to Szecket [12].

The transition zone is given for the 2024 aluminum alloy; nevertheless, the parameters corresponding to the lower limit for less perfectly cleaned surfaces ($V_w = 3000$–5000 m/s) should enable a welding without waves. These values correspond to the collision angles β between 9° and 15°. If PETN and a value of $R = 1/3$ are chosen, the range of the initial angle α will be from 5° to 10°. Fig. 3 shows the application of Eqs. (1)–(10) to the V_w vs. β space. Two different flyer plate thicknesses t are used: 1.5 and 3 mm. The smooth–wavy interface transition is shown in this plot, and two regimes are clearly seen.

3. Experiments

3.1. Experimental set-up

Fig. 4a shows the proposed capsule used in Mars Sample Return Mission. The collapse of the flyer tube upon the parent tube provides the hermetic seal of the capsule. The explosive is point-initiated and the detonation follows a circular pattern with two fronts. The angle between the two tubes is α. In order to experiment with these conditions, flat plates were tested. Indeed, Fig. 4b shows that the axial collapse and not the radial propagation is responsible for welding. The radial velocity V_{d1} is supersonic with respect to aluminum and therefore cannot promote welding. Thus, the problem was reduced to 2D in order to become tractable. One would need simultaneous initiation along the radius to create a perfect 2D configuration. The experimental set-up uses a chamfered parent plate in order to facilitate the creation of the initial angle α. These experiments have been performed with α varying between 4° and 14°. A PETN-based plastic explosive was used with a linear density of 4.25 g/m.

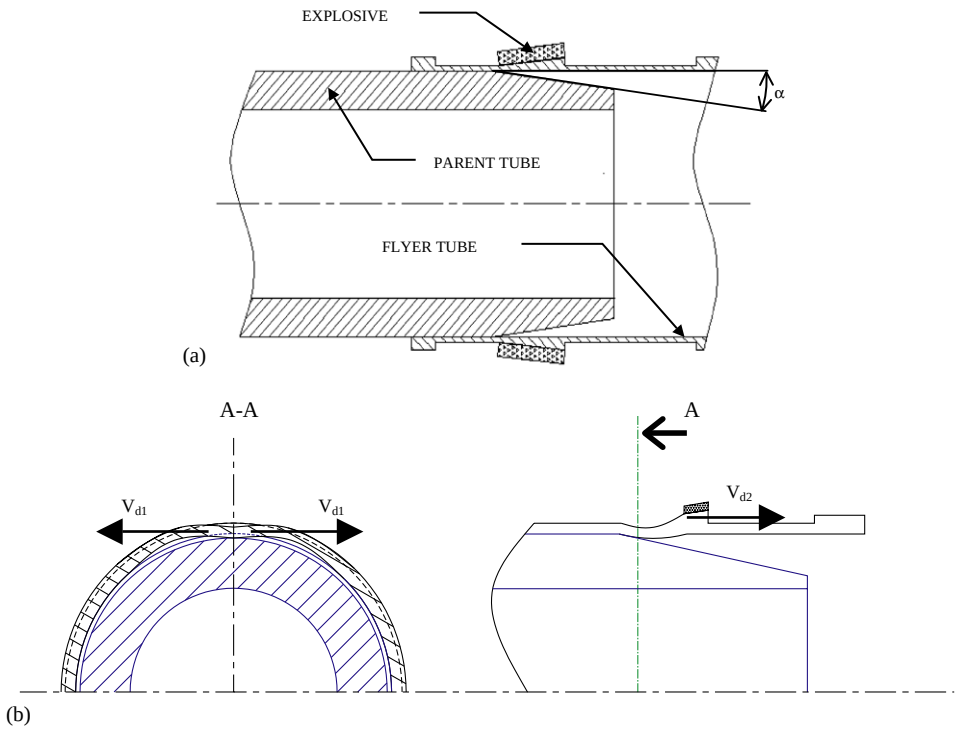

Fig. 4. (a) Configuration used in explosive welding of capsule; (b) detonation velocity V_{d2} enables welding in longitudinal direction whereas V_{d1} is too high to enable welding in the radial direction.

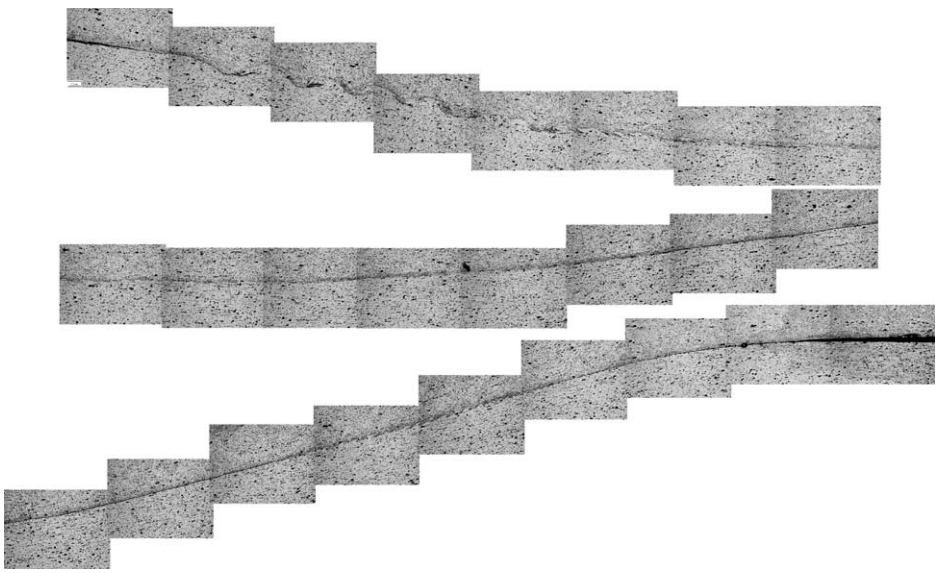

Fig. 5. Montage showing entire welded interface for $\alpha = 4^\circ$ configuration. Top: beginning of the weld. Welding from the left to the right.

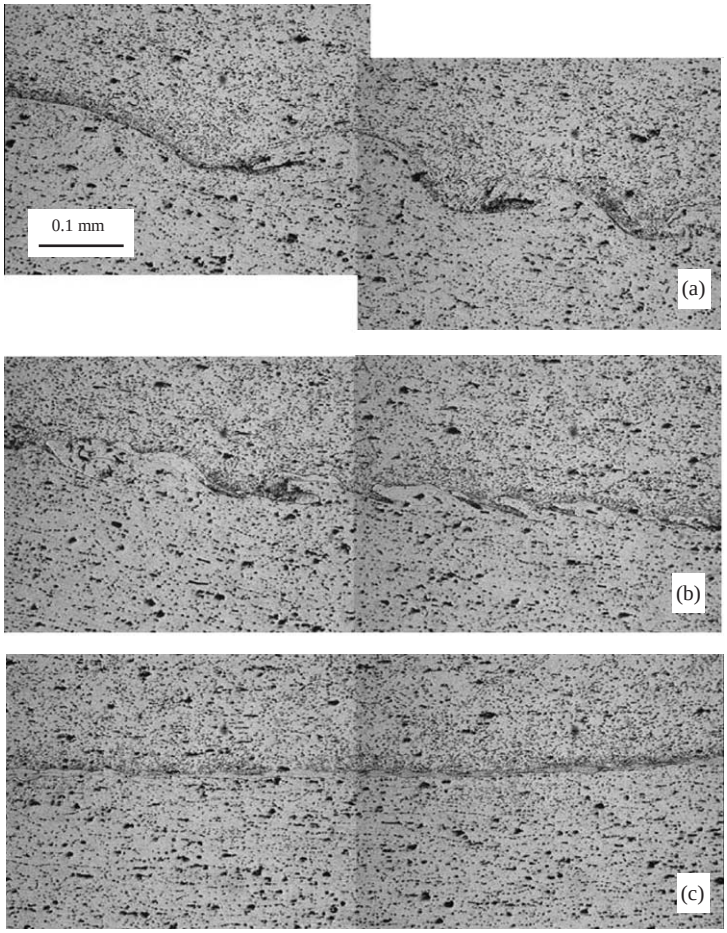

Fig. 6. Weld interface for initial angle $\alpha = 4^\circ$: (a) initial portion; (b) transition portion; (c) final portion.

3.2. Results

Experiments were carried out at initial angles of 4°, 6°, 8°, 10°, 12° and 14°. A configuration with an additional gold sacrificial layer, used as a tracer, was also tested and characterized. Fig. 5 shows a montage with the entire welding interface. Welding was initiated at the top left and terminated at the bottom right. The weld morphology is initially wavy (first 1/3) and then becomes smooth. The same pattern was observed for the other values of α. Figs. 6–8 show details from the initial, middle, and final portions of the weld for $\alpha = 4^\circ$, 8°, and 10°, respectively. There are clear differences between the wavelengths of the welds for the different values of α. Simple theoretical considerations assume (and this is the main assumption of the analytical treatment of Section 2) that explosive welding is a steady process, even at values of α different from zero. This means that, for fixed initial parameters, the interfacial geometry retains the same shape along the length of the weld. However, Fig. 5 shows that there is no stable interfacial geometry. Fig. 8 shows (marked with arrows) a void due to solidification shrinkage.

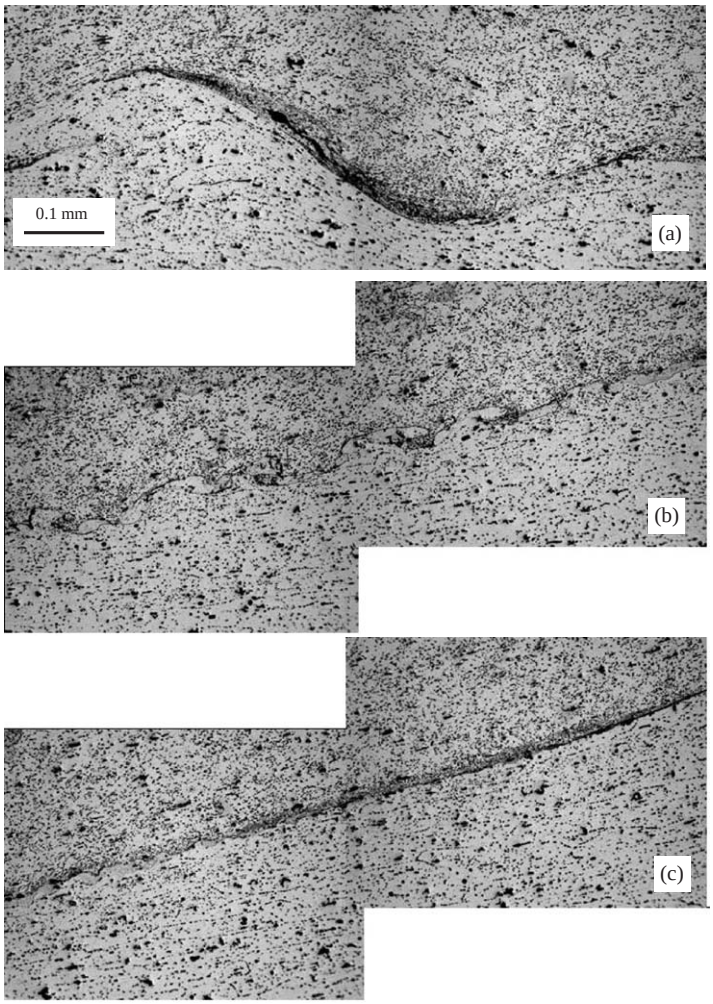

Fig. 7. Weld interface for initial angle $\alpha = 8°$: (a) initial portion; (b) transition portion; (c) final portion.

Fig. 9 shows the welded interface for the configuration in which a gold interlayer was used. The gold has been squeezed out of some regions and concentrated in other regions marked by the arrows. This experiment enabled the verification of the pulsating nature of the interface. The presence of voids from solidification shrinkage and the lower wavelength on the right are evidence of increased melting.

4. Finite element modeling

4.1. Description of the code

The finite difference and finite element communities have used Eulerian methods for over 30 years to analyze problem with explosive loading, but until comparatively recently, they were too

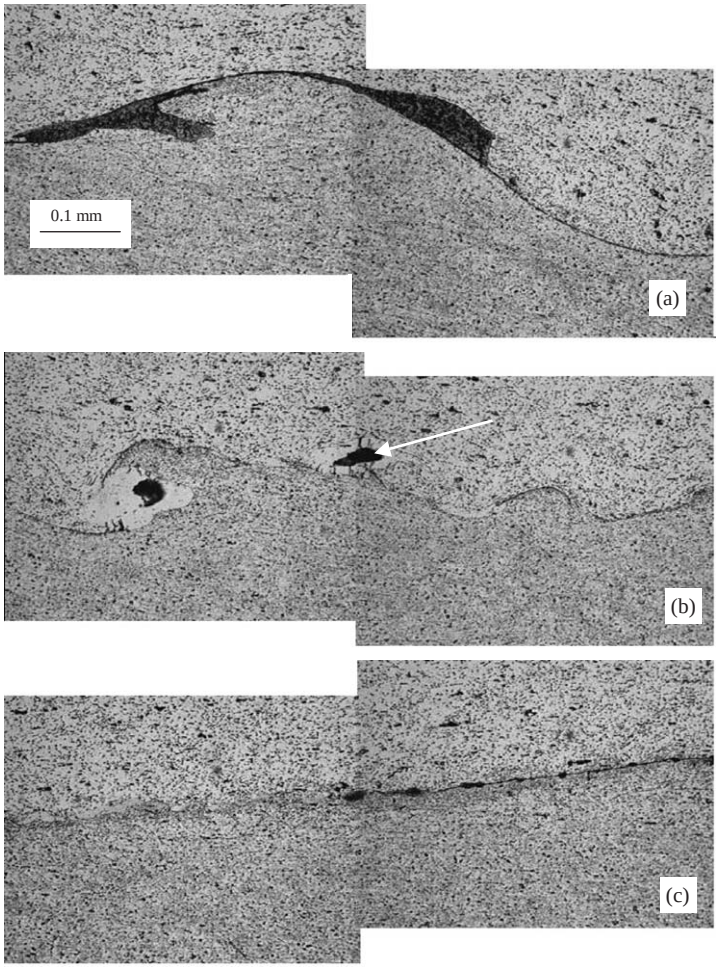

Fig. 8. Weld interface for initial angle $\alpha = 10^{\circ}$ using Au tracer at interface: (a) initial portion; (b) transition portion; (c) final portion.

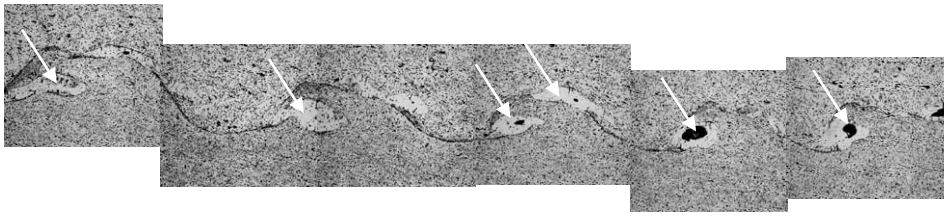

Fig. 9. Verification of pulsating nature of interface using gold interlayer ($\alpha = 10^{0}$); notice presence of voids from solidification shrinkage and lower wavelength on right.

computationally demanding and inaccurate to be attractive for solving problems in solid mechanics. The strengths and weaknesses of the Eulerian formulation are summarized here in a brief description of the computational methods used in Raven, an explicit, multi-material Eulerian program developed by David Benson [28]. The review by Benson [29] discusses the algorithms in greater detail. Benson and coworkers [30] successfully used Raven in the computation of explosive compaction and shock synthesis.

Operator splitting replaces a differential equation with a set of equations that are solved sequentially. To illustrate its application in a multi-material Eulerian code, consider Eq. (11), a simple transport equation, where φ is a solution variable, u is the velocity, and Φ is a source term.

$$\frac{\partial \varphi}{\partial t} + \vec{u} \cdot \nabla \varphi = \phi. \tag{11}$$

This equation is split into two equations,

$$\frac{\partial \varphi}{\partial t} = \phi, \tag{12}$$

$$\frac{\partial \varphi}{\partial t} + \vec{u} \cdot \nabla \varphi = 0, \tag{13}$$

where Eqs. (12) and (13) are referred to as the Lagrangian and Eulerian steps, respectively.

The Lagrangian step uses the central difference algorithm to advance the solution in time in the same manner as a standard explicit Lagrangian finite element formulation.

The Eulerian step is equivalent to a projection of the solution from one mesh onto another, and a perfect projection should be completely conservative. Most transport algorithms are conservative by construction: a flux added to one element is subtracted from its neighbor. Van Leer [31] developed the MUSCL transport algorithm used in the current calculation. The transport volumes are geometrical calculations defined by the mesh motion and they are independent of the transport kernel. The 1D algorithm is extended to 2D by performing sweeps along one mesh direction, then another sweep in the other direction.

4.2. Material models

The Johnson–Cook constitutive model [32] was used for the 6061 T0 aluminum alloy. The advantage of this equation is that the five parameters can easily be extracted from mechanical tests. The Johnson–Cook equation is

$$\sigma = (\sigma_0 + B\varepsilon^n)\left(1 + C \ln \frac{\dot{\varepsilon}}{\dot{\varepsilon}_0}\right)[1 - (T^*)^m] \tag{14}$$

with

$$T^* = \frac{T - T_r}{T_m - T_r}. \tag{15}$$

The five parameters are σ_0, B, C, n, and m. T_r is a reference temperature (at which σ_0 is measured) and $\dot{\varepsilon}_0$ is a reference strain rate (often equal to 1). The first term gives the stress as function of strain with $\dot{\varepsilon}/\dot{\varepsilon}_0 = 1$ and $T^* = 0$. The second and the third terms represent, respectively, the strain rate and the temperature effects. The values of the parameters were derived

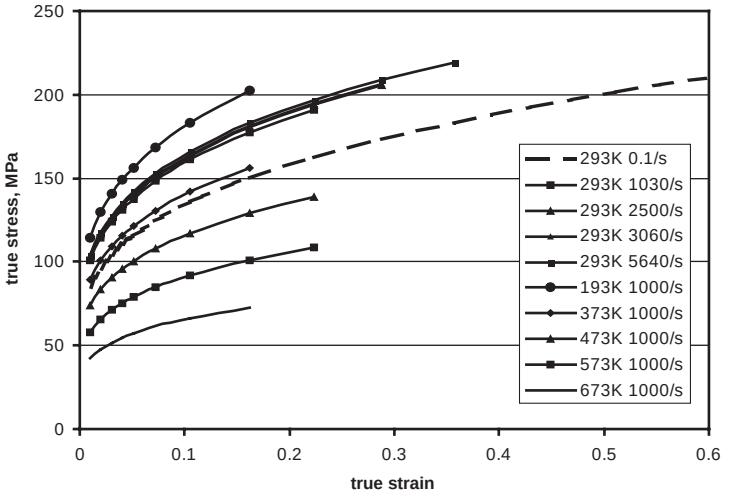

Fig. 10. Mechanical response of 6061 T0 aluminum as a function of temperature (dashed curve represents ambient temperature quasistatic response).

from quasistatic and dynamic mechanical tests carried out on the 6061 T0 aluminum alloy. The dynamic tests were conducted in a split Hopkinson bar at varying temperatures. The results of the mechanical tests are presented in Fig. 10. The JC parameters obtained from the experiments are

$$\sigma_0 = 60 \text{ MPa}, \quad n = 0.3,$$
$$B = 500 \text{ MPa}, \quad m = 1.$$
$$C = 0.02,$$

For the explosive, the Jones–Wilkins–Lee [33] equation of state was chosen to represent the expansion of the explosive products. The JWL equation of state defines pressure as function of relative volume (inverse of density), V, and internal energy per initial volume, E, as

$$P = A\left(1 - \frac{\omega}{R_1 V}\right)e^{-R_1 V} + B\left(1 - \frac{\omega}{R_2 V}\right)e^{-R_2 V} + \frac{\omega E}{V}, \tag{16}$$

where P is the pressure, V is the relative volume, E is the internal energy, ω is the Gruneisen parameter, and A, B, R_1 and R_2 are constants which satisfy the mass, momentum, and energy conservation equations.

4.3. Computational results

Fig. 11 shows a representative 2D configuration used in Raven. The dimensions are in millimeters, the time is expressed in microseconds, and colors differentiate the materials in this and subsequent figures: the explosive is yellow; the flyer plate is green; the parent plate is blue.

The computational results are presented as time sequences. Fig. 12 shows the simulation with an initial angle of approximately 10° at 7, 10, 13, 15 and 20 μs. Calculations were also run for the

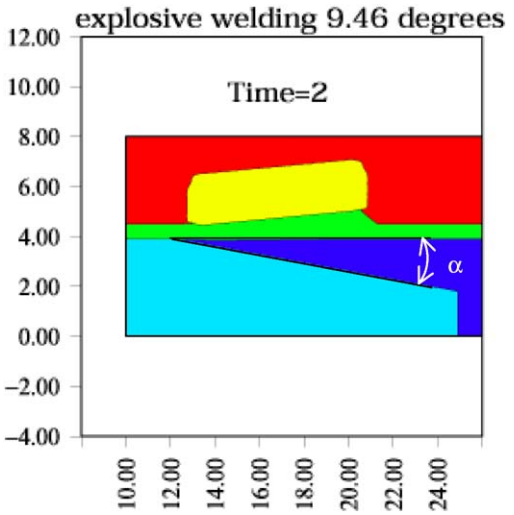

Fig. 11. 2D section used for the computations (dimensions in mm); yellow: explosive; green flyer plate; light blue: parent plate; red and blue: air.

other experimental α angles. The sequence of Fig. 12a shows that the angle β is not constant; rather, it increases with time. Fig. 12b represents a plot of collisions angles, measured from the computed welding sequences as a function of time. These measurements were made for different values of α: 4°, 6°, 7.8°, 10° and 14°. This is an important result, and it is consistent with the metallographic characterization of the weld morphology reported in Section 3. It should also be noted that the thickness of the flyer plate is not constant either, contrary to the assumptions made until now.

From the simulations it is possible to obtain the relationships between β and time, V_p and time and then, β and V_p. The results of these measurements are shown in Fig. 13 for three values of the initial angle α(4°, 8°, and 10°). The Szecket plot is superimposed on the same figure. The interfacial weld morphology is initially wavy for the three angles. As the collision angle β increases (and this angle increases with time, as shown in Fig. 12) the wavy–smooth boundary is traversed for the three cases. From that point on the welding interface is smooth. Again, this is in full agreement with the observations made in Section 3.

The computations also reveal the effect of α. The smaller α, the more rapid is the increase of β and V_p. For $\alpha = 4°$, the interface has a very short smooth–wavy transition part, and the wavelength is not constant. For $\alpha = 8°$, the interface has a large smooth–wavy transition part, and its wavelength should not be constant. Furthermore, the transition zone is reached earlier than for $\alpha = 4°$. For $\alpha = 10°$, the wavy part might be divided in two zones: the first one with decreasing wavelength as in $\alpha = 4°$ and 8°, the second one with constant wavelength. The transition region is larger than for 4° but shorter than for 8°. These predictions from the numerical results are confirmed by the experimental observations. Note also, in regard to the wave shapes, that the wavelength depends on the impact velocity V_p whereas the amplitude depends on the initial angle α. Melting appears when V_p is constant during a few microseconds (see $\alpha = 10°$).

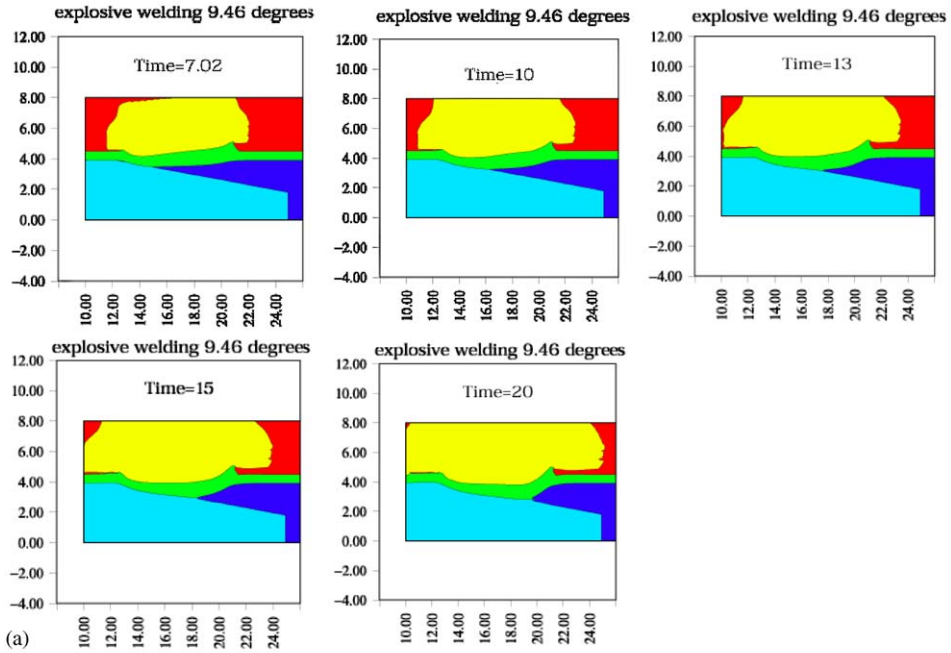

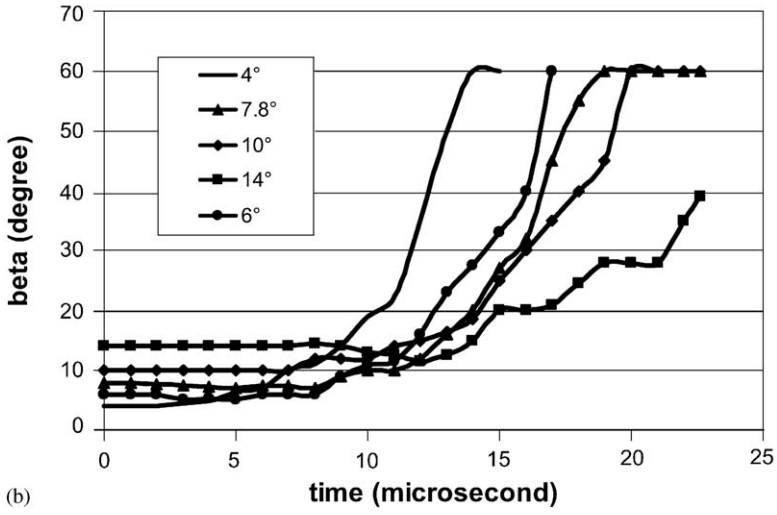

Fig. 12. (a) Numerical simulation of the explosive welding process: material behavior in function of time. Initial angle $\alpha \sim 10^{\circ}$. It should be noted that the collision angle is not a constant, but increase with weld propagation; (b) impact angle β in function of time for different values of initial angle α.

4.4. Jetting

According to the experiments of Deribas and Wittman [6], for a fixed impact velocity, V_p, the formation of the jet depends only on the value of the collision angle β. It has been shown

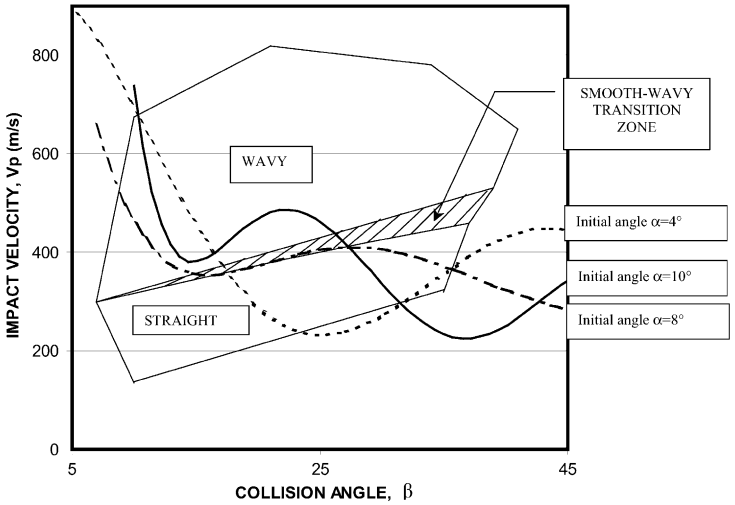

Fig. 13. Interfacial geometry as a function of the initial angle α in the β vs. V_p plane.

for the geometry studied herein that the angle is not constant during the welding process; however, the initial angle is a useful parameter for discussing our results and conclusions. For an initial angle lower than 4°, no jet is formed in the simulations. On the other hand, starting from this value, one sees a jet for each simulated configuration. It should be noted that simulations stop at 14°, an angle for which one notes a major reduction in the phenomena. The jets only form for initial angles between 4° and 15°. However, they are not created at the same time and they do not carry (at first sight), the same quantity of matter.

In Fig. 14 (configurations 8°, 10°, 12° with 25 μs), jetting first appears in the 10° configuration, and it is also the configuration for which the jet lasts the longest. One concludes from this that the quality of the welding is better at 10°. The weldability window recommends an initial angle range of 5–10° with PETN and $R = \frac{1}{3}$. All the theories suggest that when jetting occurs, it occurs during the entire welding process. Once again, this is based on a constant collision angle assumption. For Deribas [4], jetting is responsible for the formation of the waves. Unfortunately, these diagrams do not give information about the microscopic mechanisms. As one cannot see the jet along the entire welding process, the conclusion could be that it is only made with materials located on the last welded millimeter. However, Fig. 15 shows the 10° configuration with the sacrificial layer. One can observe that this third material is part of the jet.

In fact, with the current simulations, one cannot reach a reliable conclusion about the mechanism behind the formation of the waves. However, a relationship between the quantity of ejected matter and the formation of the waves seems reasonable; calculations involving a constant impact angle would help to establish this relationship. Another possibility is that when the melting temperature is reached along the interface, the wavy solid phase welding process ends, and a smooth, liquid phase welding process starts.

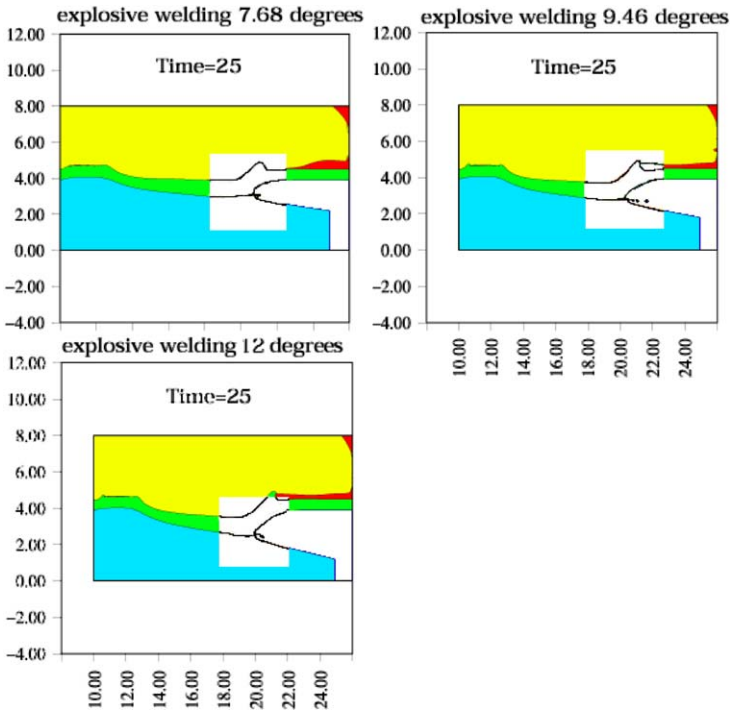

Fig. 14. Jetting at 25 μs for three different initial configurations ($\alpha \sim 8^\circ$, 10°, and 12°). Note minute points ahead of collapse region.

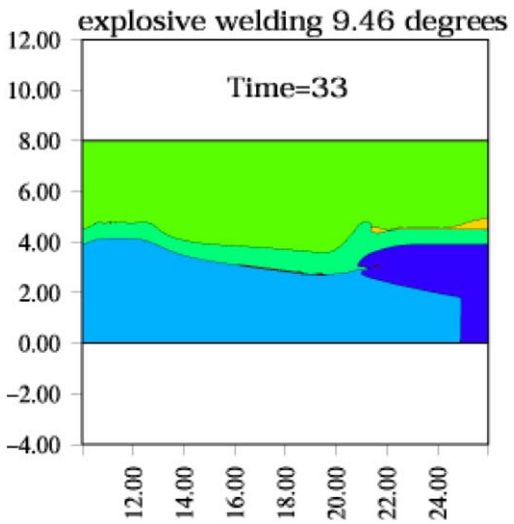

Fig. 15. $\alpha = 10^\circ$ configuration with an additional layer of Al (red material) on the flyer plate. One can see that the interlayer material forms the jet.

4.5. Bi-material welding

All the completed experiments show that the geometry of the bond depends directly on the welded materials. For a given configuration, changing one of the two metals is likely to remove the waves. Numerical simulations allow arbitrary changes in the materials without any additional expense. It is however necessary to know the Johnson–Cook parameters of the new material. For the first test, 6061 T0 aluminum alloy of the flyer plate was replaced by 6061 T6 aluminum alloy.

In the bimetal configuration, the formation of the jet appears 2 μs later, and the geometry of the jet is different. The aluminum "drops" of the second case appear bulkier but fewer than in the first. It would be interesting to examine the speed of the "drops" to obtain more precise observations.

5. Conclusions

The objective of this study was to establish the conditions for straight, smooth weld formation in the explosive welding of 6061T0 vs. 6061T0. The smooth and straight domains defined by Szecket [11] were used to successfully predict the two regimes. Szecket's [11] results for 2024 Al were supplemented by the constitutive response for 6061T0 and yielded a plot applicable to the experimental results containing both wavy and smooth domains. The present results follow Szecket's [11] calculation made for the 2024 aluminum alloy. It was possible to calculate the relationship between the terminal velocity V_p and the flyer thickness with the Gurney equation. The agreement between the calculation and the computational simulation proves that the assumption made on the flyer plate acceleration is reasonable. Experimental observations (by optical microscopy) on explosively welded specimens suggested that the V_p–β relation was not constant during the welding process since, in all cases, a region of wavy weld was followed by smooth weld. It should be noted that the thickness of the materials influences the welding process and consequently the collision angle β. For the configuration chosen for the capsules in the Mars Return Mission, the flyer plate thickness is not a constant, and thus, the impact velocity V_p should vary.

Finite element calculations using Raven were conducted in a 2D geometry. The Johnson–Cook constitutive equation was used with experimentally obtained constitutive parameters for 6061T0 Al obtained from quasistatic and dynamic experiments carried out over a broad range of temperatures. From a numerical point of view, the results are particularly convincing. However, it is manageable to reach a higher level of accuracy utilizing a model that would include higher rate sensitivity. Although the individual wave formation could not be monitored because of mesh size limitations, the results demonstrate that the collision angle increases with propagation distance for all initial configurations analyzed. This change in collision angle is directly responsible for the change in interface morphology from wavy to smooth at the welding front. Furthermore, the correlation between the experiments and the simulations demonstrates that the model is good enough to simulate the process.

The numerical simulation shows the formation of a jet under some initial conditions but does not reproduce the micromechanics of the process. The wave formation occurs on a micrometer scale that cannot be captured by the continuum mechanics computation. Nevertheless, jet formation was observed for 8°, 10°, and 12°.

Acknowledgements

The funding of this program by the Jet Propulsion Laboratory through Dr. Mark Adams is gratefully acknowledged. Frequent discussions with Dr. Benjamin Dolgin and Joseph Sanok are greatly appreciated.

We dedicate this manuscript to Professor Werner Goldsmith, a pioneer in the field of impact engineering. Like an entire generation of researchers studying dynamic phenomena of materials, we became acquainted to Professor Goldsmith through his book "Impact", first published in 1960. In the case of MAM, this was through a photocopy that circulated as a text at the Military Institute of Engineering, in Brazil (1974). We came to know Werner personally in the late 90's and early 00's. It is then that we truly appreciated his full qualities. He contributed significantly to an US Army sponsored research program on ultradynamic performance materials. His boundless energy was not slowed by his physical ailments, and he dedicated himself with great enthusiasm to the tasks of educating us in impact phenomena, carrying out experiments on his Berkeley powder gun, and correcting our frequent mistakes and misconceptions. He was a mentor to us, advising and guiding us. Our lives, as well as those of so many other colleagues, have been enriched by his presence. Adversity was present in his life all the way from childhood, when he was sent to the US. Alas, his family perished in the holocaust of WW2. He struggled through school, working his way to support himself. He joined UC Berkeley, and rose to the highest academic level, receiving the prestigious Berkeley citation and being elected to the National Academy of Engineering. Later in life, he was struck by a debilitating disease that caused him great pain and discomfort. Nevertheless, he kept pushing ahead, with admirable determination. He will live through the legacy of his scientific accomplishments and human connections.

References

[1] Dolgin B, Sanok J, Sevilla D, Bement L. Category V compliant container for Mars Sample Return Missions. 00ICES-131 2000.
[2] Birkhoff G, MacDougall DP, Pugh EM, Taylor G. Explosives with lined cavities. J Appl Phys 1948;19:563–82.
[3] Deribas AA. Explosive welding. Siberian branch of academy of sciences 1967 in explosive welding. Fiz Goreniya Vzryva 1967;3(4):561–8.
[4] Crossland B. Explosive welding of metals and its applications. Oxford: Oxford Science Publication; 1982.
[5] Meyers MA. Dynamic behavior of materials. New York: Wiley Interscience; 1994.
[6] Wittman RH. The influence of collision parameters on the strength and microstructure of an explosion welded aluminum alloy. Proceedings of the Second International Symposium on the Use of Explosive Energy in Manufacturing, Marianskie Lazni (Czechia), 1973. p. 153–68.
[7] Deribas AA, Simonov VA, Zakcharenko ID. Investigation of the explosive parameters for arbitrary combinations of metals and alloys. Proceedings of the Fifth International Conference on High Energy Rate Fabrication. 1975. p. 4.1.1–24.
[8] Deribas AA, Kudinov VM, Matveenkov FI, Simonov VA. Explosive welding. Fiz Goreniya Vzryva 1967;3(1): 111–8.
[9] Cowan GR, Holtzman AH. Flow configuration in colliding plates: explosive welding. J Appl Phys 1963;34:928–39.
[10] Cowan GR, Bergman OR, Holtzman AH. Mechanism of bond zone wave formation in explosion-clad metals. Met Trans 1971;2:3145–55.
[11] Jaramillo D, Szecket A, Inal OT. On the transition from a waveless to a wavy interface in explosive welding. Mater Sci Eng 1987;91:217–22.

[12] Szecket A. An experimental study of the explosive welding window. PhD, thesis, Queen's University of Belfast, 1979.
[13] Szecket A, Mayseless M. The triggering and controlling of stable interfacial conditions in explosive welding. Mater Sci Eng 1983;57:149–54.
[14] Szecket A, Inal OT, Vigueras DJ, Rocco J. A wavy versus straight interface in the explosive welding of aluminum to steel. J Vac Sci Technol 1985;3(6):2588–93.
[15] Szecket A, Vigueras DJ, Inal OT. The cyclic pressure distribution of explosively welded interfaces. In: Murr LE, Staudhammer KP, Meyers MA, editors. Metallurgical applications of shock-wave and high-strain-rate phenomena. New York: Dekker; 1996. p. 887–903.
[16] Deribas AA, Kudinov VM, Matveenkov FI. Effect of the initial parameters on the process of wave formation. Fizika Goreniya Vzryva 1967;3(4):561–8.
[17] Deribas AA, Kudinov VM, Matveenkov FI, Simonov VA. Simulation of the process of wave formation in explosive welding. Fiz Goreniya Vzryva 1968;4(1):100–7.
[18] Bahrani AS, Black TJ, Crossland B. The mechanics of wave formation in explosive welding. Proc Roy Soc A 1967;296(9):123–36.
[19] Reid SR. A discussion of interface wave generation in explosive welding. Int J Mech Sci 1974;16:399–413.
[20] Reid SR, Sherif NHS. Prediction of the wavelength of interface waves in symmetric explosive welding. J Mech Eng Sci 1976;18(2):87–94.
[21] Reid SR. Wake instability mechanism for wave formation in explosive welding. Int J Mech Sci 1978;20:247–53.
[22] Gupta RC, Kainth GS. Swinging wake mechanism for interface wave generation in explosive welding of metals. Trans ASME. J Appl Sci 1990;57:514–21.
[23] Gelman AS, Pervukhin LB, Tsemakhovich BD. Purification of the surfaces in the process of explosion welding. Combus Explos Shock Waves 1974;10:245–8.
[24] Simonov VA. Binding criterion for metals with explosive welding. Fiz Goreniya Vzryva 1991;27(1):127–30.
[25] Simonov VA. The relationship between plastic deformation and collision angle in explosive welding. Fiz Goreniya Vzryva 1991;27(3):91–4.
[26] Simonov VA. Additional limitations on the explosive welding. Fiz Goreniya 1991;28(1):110–4.
[27] Gurney R. The initial velocities of fragments from bombs, shells, and grenades. Report No. 405, Ballistic Research Laboratory, Aberdeen, MD, September 1943:AII-36218.
[28] Benson DJ. RAVEN: User's Manual ver 2000.
[29] Benson DJ. Computational methods in Lagrangian and Eulerian hydrocodes. Comp Meth Appl Mech Eng 1992;99:235.
[30] Meyers MA, Benson DJ, Olevsky EA. Shock consolidation: microstructurally-based analysis and computation modeling. Acta Mater 1999;47(7):2089–108.
[31] Van Leer B. Comp. Towards the ultimate conservative difference scheme IV. A new approach to numerical convection. Physica 1977;23:276.
[32] Johnson GR, Cook WH. A constitutive model and data for metals subjected to large strains, high strain rates and high temperatures. Presented at the Seventh International Symposium on Ballistics, The Hague, Netherlands, 1983.
[33] Dobratz BM. Explosives handbook: properties of chemical explosives and explosives simulants. UCRL-52997, Lawrence Livermore National Laboratory, Livermore, CA, 1981.